Materials Advances

ROYAL SOCIETY OF CHEMISTRY

PAPER

View Article Online
View Journal | View Issue

Cite this: *Mater. Adv.*, 2024, 5, 4857

Unveiling $BiVO_4$ photoelectrocatalytic potential for CO_2 reduction at ambient temperature†

Ricardo Marques e Silva,[ab] Eduardo Henrique Dias,[ac] Florymar Escalona-Durán,[ad] Gelson Tiago dos Santos Tavares da Silva,[e] Wajdi Alnoush,[b] Jessica Ariane de Oliveira,[a] Drew Higgins[b] and Caue Ribeiro *[a]

Received 8th March 2024,
Accepted 14th April 2024

DOI: 10.1039/d4ma00232f

rsc.li/materials-advances

Here, we explore monoclinic $BiVO_4$ as a cathode in a photoelectrochemical (PEC) system for CO_2 reduction (CO_2R). The catalyst was prepared using a simple oxidant peroxide method with crystallization under hydrothermal conditions, and subsequently sprayed on the FTO substrate. CO_2R was carried out in an inflow and sealed electrochemical system for 6 h. The best performance was found to be under photoelectrocatalysis powered by a light-emitting diode (LED) as an illumination source when compared to photocatalysis (using different halogen UV and LED illumination), electrocatalysis, and photoelectrocatalysis powered by a halogen UV illumination source, with total production values of 22 and 5.5 μmol cm^{-2} for methanol and acetic acid, respectively. This achievement occurs because, even though $BiVO_4$ as a photocatalyst does not have sufficient potential to drive CO_2R, an external potential can be applied to drive the reaction. Moreover, the photogenerated electron–hole pairs are guided by the external potential, improving the charge separation and promoting the rapid electron transfer to reduce CO_2 on the photoelectrocathode at a lower overpotential when compared to electrocatalysis. LED illumination produced higher amounts of products than UV illumination because UV light affects the catalyst surface altering the number of catalytic sites available for the reaction and reducing their performance.

1. Introduction

The utilization of fossil fuels causes the generation of greenhouse gases, especially carbon dioxide (CO_2), motivating the development of novel technologies to convert them into value-added chemicals.[1] In this context, photoelectrochemical (PEC) conversion arises as a promising technology for carbon dioxide reduction (CO_2R).[2,3] Although photocatalysis by itself suffers from limited utilization efficiency of solar energy and low separation of photogenerated carriers, it can support electrocatalysis by decreasing the amount of electrode potential that must be applied to promote the reaction. Indeed, more negative potentials lead to the occurrence of competing electrochemical reactions, reducing the overall efficiency of the system.[4] A typical PEC system for CO_2R consists of a semiconductor photoelectrode as the main component, which is usually dual-functional; it facilitates both the absorption of light and the electrochemical CO_2R. This technology leverages the abundant photon energy from sunlight, an infinite natural resource. It combines this energy with an applied electrochemical potential to serve as a driving force, effectively regulating the electronic flow within the system. This integrated approach eliminates the necessity for high temperatures and voltages, capitalizing on the strengths of both photon and electron technologies. By improving the efficiency of charge transfer and reducing unwanted side reactions, this technology enables active and selective reduction of CO_2 to fuels and valuable chemicals, where selectivity is fine-tuned by controlling the primary reaction stages.[4–6]

To this end, efficient catalysts are essential to improve the CO_2R performance. The ideal catalyst should be cost-effective, having an optimum band gap and high efficiency in the range of visible light, allowing it to efficiently absorb visible light and generate electron–hole pairs.[7] Bismuth vanadate ($BiVO_4$) is a candidate that meets these requirements, specifically due to its band gap of 2.4 eV. Additionally, $BiVO_4$ is thermodynamically stable in its monoclinic phase, presents good chemical stability, and is composed of relatively inexpensive elements.[8] However, there is a lack of studies on pristine $BiVO_4$ used as a cathode photoelectrocatalyst for CO_2R.

[a] Nanotechnology National Laboratory for Agriculture (LNNA), Embrapa Instrumentation, São Carlos, São Paulo, Brazil. E-mail: caue.ribeiro@embrapa.br
[b] Department of Chemical Engineering, McMaster University, Hamilton, Ontario L8S 4L7, Canada
[c] Institute of Chemistry (IQSC), University of São Paulo, São Carlos, São Paulo, Brazil
[d] Department of Fuel and Hydrogen Cells (CECCO), Nuclear and Energy Research Institute (IPEN), São Paulo, São Paulo, Brazil
[e] Interdisciplinary Laboratory of Electrochemistry and Ceramics, Department of Chemistry, Federal University of São Carlos, São Carlos, São Paulo, Brazil

† Electronic supplementary information (ESI) available. See DOI: https://doi.org/10.1039/d4ma00232f

Here, a monoclinic $BiVO_4$ was synthesized by a simple oxidant peroxide method with crystallization under hydrothermal conditions. Electrodes were then prepared by spray coating $BiVO_4$ on a fluorine-doped tin oxide-coated glass (FTO) substrate. The electrodes ($BiVO_4$/FTO) were used as cathodes under either UV or LED irradiation in a photocatalytic approach, with results compared to electrocatalytic and photoelectrocatalytic setups. Photoelectrocatalysis using LED illumination as an excitation source was found to provide the best performance, exhibiting total production values of 22 and 5.5 μmol cm^{-2} for methanol and acetic acid, respectively. LED illumination produced higher amounts of methanol and acetic acid than the UV illumination as an excitation source although the UV illumination carries more energy per photon than the LED. It is worth noting that most studies on $BiVO_4$ have focused on its use as a photoanode, with relatively fewer studies investigating its potential as a cathode material; exploring its potential as a cathode presents the advantage of forming a heterojunction on the catalyst surface, induced by the external negative potential applied. Thus, this study emphasizes the use of $BiVO_4$ as a cathode photoelectrocatalyst for CO_2R and led to important findings for future applications regarding advanced sustainable technologies for CO_2 mitigation.

2. Experimental

2.1. Materials

The chemicals, bismuth(III) nitrate pentahydrate $(BiNO_3)_3{\cdot}5H_2O$, ammonium metavanadate (NH_4VO_3), sodium bicarbonate ($NaHCO_3$), hydrogen peroxide (H_2O_2, 30% concentration), and anhydrous alcohol, were of analytical grade and were used as received from Sigma Aldrich. For the preparation of all solutions, type I ultrapure water (Millipore Milli-Q system, with a resistivity of 18.2 MΩ cm at 25 °C), was utilized. Nitrogen (N_2) and carbon dioxide (CO_2) gases, both with a purity of 99.99%, were purchased from White Martins Inc. (Brazil). For the proper electrode deposition, a 5 wt% alcohol-based dispersion (Nafion™ D521, Fuel Cell Store, USA) was used as a binding material. Fluorine-doped tin oxide coated glass (FTO – 2.2 mm) having a surface resistivity of approximately 7 Ω sq^{-1} was purchased from Sigma Aldrich.

2.2. Synthesis and electrode preparation

The catalysts were synthesized by adding 0.345 g of $Bi(NO_3)_3{\cdot}5H_2O$, 0.08 g of NH_4VO_3, 100 mL of H_2O, and 110 μl of H_2O_2 to the Teflon lining, which was inserted into the stainless steel vessel and stirred at room temperature (25 °C) for 30 min. The vessel was then sealed and heated hydrothermally at 160 °C for 720 min with a heating rate of 3 °C min^{-1}, as reported in ref. 9. After the synthesis was complete, the yellow solid powder was washed and centrifuged with anhydrous alcohol three times and dried overnight at 50 °C. Prior to catalyst deposition, the FTO substrate was cleaned in the following sequence: first with type I ultrapure water and Extran® soap under sonication for 5 min, then with anhydrous alcohol under sonication for 5 min, followed by acetone under sonication for 5 min, and further cleaned with type I ultrapure water under sonication for 5 min to remove impurities. Finally, the cleaned substrate was dried using N_2 flux. Electrodes were prepared based on our previous work[10,11] by spray-coating the catalyst to form a thin film on the FTO substrate (dimensions 2.5 × 2 cm for an area of 5 cm^2). For every deposition, a slurry of catalyst was created by blending 25 mg of the catalyst with 25 mL of isopropanol and 0.25 mL of Nafion™. This mixture was ground using a mortar and pestle for 20 min. Following this, the slurry was dispersed in an additional 100 mL of isopropanol and sonicated for 30 min. The resulting suspensions were then sprayed to achieve a loading of 3.0 ± 2 mg cm^{-2} on FTO that was placed on a heating plate set to 60 °C to expedite the evaporation of the solvent.

2.3. Characterization

The crystal phase of the prepared $BiVO_4$ powders was determined using X-ray diffraction (XRD, Shimadzu XRD-6000 diffractometer model) with a Cu Kα radiation source (λ = 1.5418 Å) operating at 30 kV and 30 mA. Data were collected at diffraction angles between 10° and 80° at a scan rate of 2° per minute. The identification of the phase was based on JCPDS cards, and the primary crystallite size was calculated using Scherrer eqn (1).[12]

$$d = \frac{0.9\lambda}{B\cos\theta} \quad (1)$$

where λ is the X-ray wavelength corresponding to the Cu Kα radiation (0.15406 nm), θ is the diffraction angle and B is the line broadening (in radians) at half of its maximum (FWHM). To supplement the data on phase identification and structural analysis, Raman spectra were collected (Raman, Horiba LabRam HR Evolution) using a laser excitation wavelength of 532 nm within a range from 100 to 1000 cm^{-1}. X-Ray absorption spectroscopy (XAS) was carried out at the hard X-ray micro-analysis (HXMA) beamline at the canadian light source (CLS). X-Ray near edge spectroscopy (XANES) and extended X-ray fine structure (EXAFS) spectra were collected at the Bi L_3-edge (13.418 keV) in the transmission mode for the $BiVO_4$ photoelectrocatalyst pre- and post-reaction. The morphologies, crystalline structures, and chemical compositions of the catalysts were examined using a field emission scanning electron microscope (FEG-SEM, JEOL 6700) and a scanning transmission electron microscope (STEM, FEI Tecnai G2 F20) equipped with high-resolution imaging (HRTEM) and energy-dispersive X-ray (EDX) capabilities. Each sample was prepared by dispersing a colloidal alcoholic suspension on a carbon-coated copper grid and allowing it to dry before microscopic measurement. The Tauc method[13] was applied to calculate the indirect band gap energy of each sample using the diffuse reflection spectrum (DRS, Shimadzu UV-2600 spectrophotometer). The photoluminescence (PL) measurements were conducted using a laser source with an excitation wavelength of 355 nm, maintaining a steady power of 5 mW focused on a 200 μm spot. The luminescence signal was dispersed using an Andor/Kymera 19.3 cm spectrometer and captured using an Andor/Idus BU2 Si charge-coupled device. Nitrogen adsorption–desorption isotherms and Brunauer–Emmett–Teller (BET) specific surface areas were determined using a Micromeritics ASAP 2020

instrument at −196 °C. Liquid products were identified and quantified using a ^{1}H Nuclear Magnetic Resonance (NMR, Bruker Ascend™ 600 MHz) operating at 25 °C. Each sample, consisting of 540 μL aliquots, was combined with a solution containing 60 μL of D_2O, 50 mM of standard dimethyl sulfoxide (DMSO), and 0.21 mM of reference 3-(trimethylsilyl)propionic-2,2,3,3-d4 acid sodium salt (TSPd4). The water peak was suppressed using the WET method, and the raw NMR data were analyzed using MestReNova software.

2.4. Flow cell configuration

The CO_2R experimental setup was designed using a custom-made filter-press PEC reactor with an inflow and a sealed system – the continuous-flow system was used to overcome mass transfer limitations caused by low solubility and slow diffusion of CO_2 in water. This lab-scale setup includes jacketed glass tanks for anolyte and catholyte, each with a capacity of 100 mL, connected to a thermostatic bath. It also features peristaltic pumps for fluid recirculation through the photoelectric reactor. Depending on the desired illumination source, a 100 W halogen lamp for UV-Vis light (UV) or a 100 W light-emitting diode (LED) lamp for visible light can be used (more details on the light spectrum in Fig. S1, ESI†). The setup also consists of a two-chamber PEC flow cell, separated by a cation exchange membrane (Nafion 117), and Ag/AgCl 3.0 M KCl as a reference electrode. All fluid connections were positioned on the side plate of the reactor. Each experiment was conducted employing different types of excitations on the electrodes. Photon reactions were performed solely by employing UV or LED irradiation exclusively at the cathode (*i.e.*, the anode was always in the dark). Electrochemical reactions were performed only by employing an applied potential. Photoelectron reactions were performed with light irradiation and applied potential simultaneously. It is important to mention that the experimental preparation process remained equivalent for all reactions, except for the different excitation sources mentioned above. The cathodic and anodic chambers contain 3.2 mL each, while the reservoirs held a reaction volume of 100 mL of 0.5 M $NaHCO_3$ electrolyte with a pH of 8. Before the experiments, the catholyte was purged with a constant flow of N_2 at a flow rate of 30 mL min^{-1} for 20 min, followed by saturation with CO_2 at a flow rate of 30 mL min^{-1} for 30 min. Cyclic voltammetry was performed under the aforementioned conditions, applying a potential window from 0.1 to −1.5 V *vs.* Ag/AgCl at a sweep rate of 20 mV s^{-1} with LED illumination, as an irradiation source. Thus, a −1.0 V *vs.* Ag/AgCl was set as the potential to favor CO_2R, avoiding the hydrogen evolution reaction (Fig. S2, ESI†). For electrochemically driven reactions, chronoamperometric measurements were taken at −1.0 V *vs.* Ag/AgCl, controlled using an Autolab potentiostat (Multi Autolab/M204). Photon-driven reactions were carried out using either a UV or LED light source, while photoelectrochemical reactions were measured both chronoamperometrically at −1.0 V *vs.* Ag/AgCl and a UV or LED source simultaneously. All experiments were performed with recirculation through the reservoir and the PEC reactor was maintained at a flow rate of 14 mL min^{-1}.

3. Results and discussion

The structure and morphology of the as-synthesized $BiVO_4$ (Fig. 1) were imaged using electron microscopy. Fig. 1(A) represents the SEM micrographs which displayed nanometer and micrometer size particles in a range from 0.02 to 2 μm with sphere-like and worm-like shapes in large aggregates, possessing a low surface area of 1.5913 m^2 g^{-1} (Fig. S3, ESI†). The particle size and shape are controllable by changing the H_2O_2 concentration used during synthesis as this affects the nucleation step and growth process, as previously studied by Lopes *et al.*, 2016.[9] This is important since the efficient charge separation in the PEC system achieves its effectiveness through the use of small particles – unlike photocatalysis – which leads to a reduced hole diffusion length and better interparticle and particle/substrate contacts. Fig. 1(B) shows a TEM image of the $BiVO_4$ particles, revealing agglomerates formed from a large number of well-faceted particles with an interplanar distance of 4.1 Å in relation to the plane (112) to the monoclinic phase, as shown in Fig. 1(D). Furthermore, the high-resolution TEM image shows clear lattice spacing, indicating good crystallinity of the $BiVO_4$ nanoparticles. Fig. 1(C) shows the TEM-EDX analysis that identifies the presence of uniformly distributed Bi, O, and V particles.

The electronic properties of the prepared $BiVO_4$ sample are shown in Fig. 2. The band gap edge showed the typical absorption shape found for $BiVO_4$ single particles.[14] The band gap of the crystalline semiconductor was calculated from the Tauc equation (2) as follows:

$$\alpha h\nu = A(h\nu - E_g)^{1/n} \quad (2)$$

where α, h, ν, A, and E_g denote the absorption coefficient, Planck constant, frequency of vibration, proportional constant, and band gap, respectively. However, the value of the exponent n denotes the nature of the semiconductor, whereby for direct

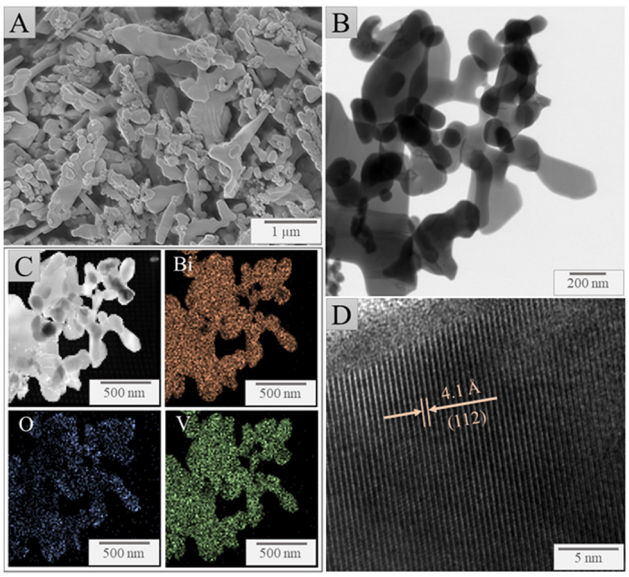

Fig. 1 Electron micrographs of the as-synthesized $BiVO_4$, (A) SEM image, (B) TEM image, (C) TEM-EDX, (D) HRTEM image.

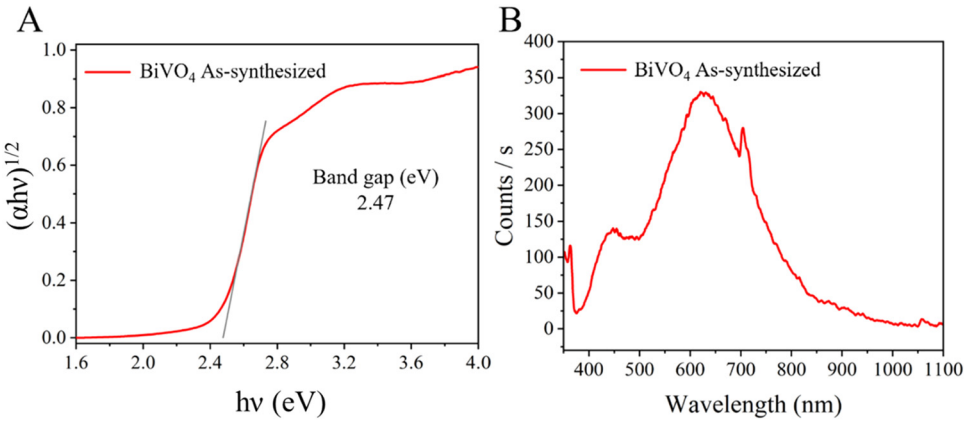

Fig. 2 (A) Tauc plot (indirect band gap value) and (B) photoluminescence (PL) spectrum of the as-synthesized $BiVO_4$.

and indirect transition allowed, n is 1/2 and 2, respectively. As a result, the estimated E_g for the indirect electron transition from the Bi 6s or hybrid Bi 6s–O 2p valence band to the V 3d energy level of the prepared $BiVO_4$ was 2.47 eV (Fig. 2(A)), suggesting that the obtained material matches pure monoclinic $BiVO_4$, a material with good visible-light-driven proprieties.[15] Fig. 2(B) depicts the PL spectrum of produced $BiVO_4$ samples with an excitation wavelength of 355 nm. This finding shows that the $BiVO_4$ sample contains two emission peaks. The peak at *ca.* 650 nm is attributed to the recombination of electrons in the conduction band of the V 3d orbital to holes formed in the valence band of the O 2p orbital, whereas the peak at *ca.* 450 nm is attributed to the recombination of some extrinsic radiation transitions, such as recombination of charges related to defects or impurities in the crystal structure.[16]

The current density *versus* applied potential curves for the electrocatalytic and PEC reactions (Fig. S2, ESI†) exhibited a noticeable difference in the current response, indicating better separation of the photogenerated charges by the PEC reaction system. The total production of liquid chemicals from CO_2R of as-synthesized $BiVO_4$ for all different excitation sources – that is, for photocatalysis (using different UV and LED illumination sources), electrocatalysis (using chronoamperometric measurements at −1.0 V *vs.* Ag/AgCl), and photoelectrocatalysis (using both photos, using UV or LED illumination, and chronoamperometric measurements at −1.0 V *vs.* Ag/AgCl as a source – were measured *via* ^{1}H-NMR, as shown in Fig. 3).

Photocatalysis on its own was not effective in promoting CO_2R because although the photocatalyst ($BiVO_4$) has a favorable band gap in the visible range (2.4 eV–516 nm), its electronic and surface structure is not conducive to driving the CO_2R reaction; in particular, its conductive band is thermodynamically unfavorable to produce $CO_2^{\bullet-}$ intermediates, and the inherent high density of surface recombination further hinders the CO_2R.[17] Regarding the production of liquid chemicals from CO_2R by electrocatalysis, the liquid production exhibited low amounts of methanol (2.1 μmol cm^{-2}), acetate (0.14 μmol cm^{-2}), and other byproducts but in low amounts, which are below the confidence level. It is proposed that the product selectivity is associated with Bi–$BiVO_4$ heterojunctions,

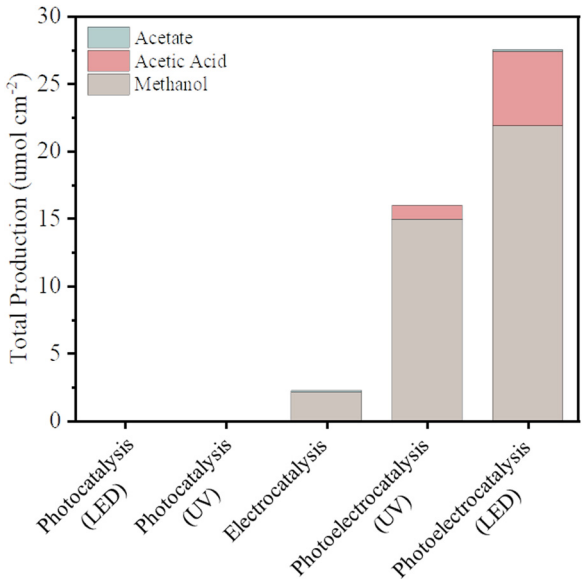

Fig. 3 Total production of liquid chemicals from CO_2R using as-synthesized $BiVO_4$ as catalysts and induced by photocatalysis (using different UV and LED illumination), electrocatalysis, and photoelectrocatalysis (using both electrons and photons by UV or LED illumination) sources. The reactions were made in 0.5 M $NaHCO_3$ at pH 8 for 6 h. Prior to the reactions, the electrolyte was purged with CO_2 gas. A 100 W halogen lamp (UV-Vis light) and a 100 W light-emitting diode lamp (LED-Vis light) were used as a source for photon-driven reactions, chronoamperometric measurements at −1.0 V *vs.* Ag/AgCl was employed for the electrocatalytic reactions, and both photo (UV or LED illumination) and chronoamperometric measurements (at −1.0 V *vs.* Ag/AgCl) source were applied for photoelectron reactions. All experiments were performed with recirculation through the reservoir. More details are found in the flow cell configuration section.

which can be formed by Bi-metallic on the $BiVO_4$ surface when a negative potential of −1.0 V *vs.* Ag/AgCl is applied.[18–20] This hypothesis is based on the potential-pH equilibrium diagram for Bi, which shows that, in any cathodic region below Hydrogen evolution potential, metallic Bi is stably formed. On the other hand, in the same potential range, it is expected that V_2O_3 is still stable, as shown in Fig. 4.

Indeed, both the Bi–$BiVO_4$ heterojunction and the external potential applied would contribute to addressing the

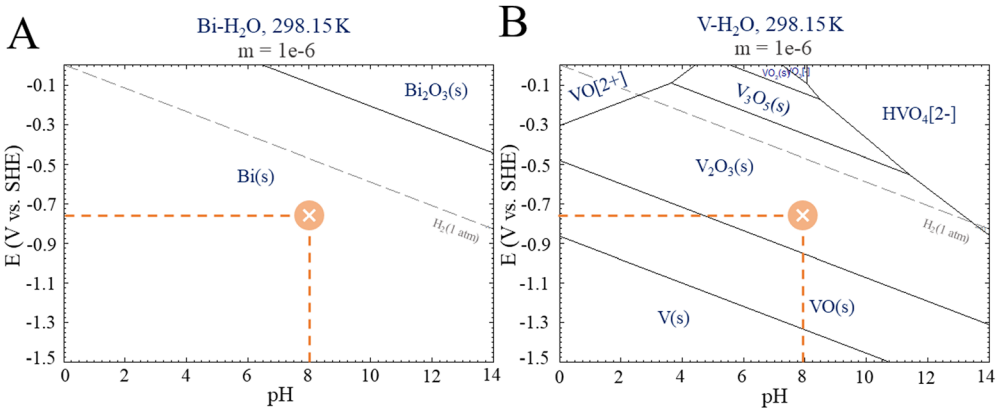

Fig. 4 E-pH diagrams from Pourbaix for (A) Bismuth and (B) Vanadium. Adapted from the Centre for Research in Computational Thermochemistry (CRCT).[22]

recombination rate issue by the internal electric field and fine-tuning of redox potentials, respectively.[21] The low production of liquid products can be justified by the energy barrier between the valence and conduction bands, which are characteristic of a semiconductor. This could be boosted by increasing the applied external potential; in a more negative direction in this instance. However, this approach can lead to the formation of undesired products, such as hydrogen.

Photoelectrocatalysis demonstrated superior performance compared to standalone photocatalysis and electrocatalysis since it combines aspects of both methods. In this context, instead of increasing the external potential in a more negative direction, which could lead to the issues mentioned, a light source was integrated into the system. This integration promotes the generation of electron–hole pairs on the catalyst; through light absorption, which in turn are guided by the external potential. This enhancement in charge separation efficiency facilitates rapid electron transfer, resulting in a more efficient reduction of CO_2 keeping the same potential used in the electrocatalysis method.[4,19] Comparing the two illumination sources in photoelectrocatalysis, the results under LED illumination were better than the results powered by UV illumination – exhibiting total production of methanol (22 μmol cm^{-2}), acetic acid (5.5 μmol cm^{-2}), and other byproducts such as acetate (0.13 μmol cm^{-2}) but in low amounts, which are below the confidence level (for reference, see Fig. S4, ESI†). This result is noteworthy since UV irradiation carries more energy per photon than LED irradiation, allowing it to deliver a greater amount of energy to the catalyst and, hence, an increase in its electronic excitation.[23] On the other hand, UV light can affect the catalyst surface due to photo-induced reactions, with emphasis on the surface properties including defects, roughness, and oxygen vacancies. These features contribute to the number of catalytic sites available for the reaction to occur, as well as the reactivity of the surface. In the specific case of $BiVO_4$, UV light exposure has been shown to decrease the surface roughness and increase the smoothness of the surface, which can also have a negative effect on the catalytic potential of the catalyst when used alongside a reaction. When the surface becomes smoother, the number of catalytic sites available for the reaction decreases, which can lead to a reduction in catalytic activity.[24]

To understand the catalyst stability, a structural analysis was performed on both the as-synthesized catalyst and the post-reaction (post-CO_2R) using a photoelectrocatalyst under LED illumination as an excitation source. The crystalline phase and composition of the as-synthesized $BiVO_4$ were investigated by XRD patterns, as shown in Fig. 5(A). The diffraction peaks showed a crystalline phase with an estimated average crystallite size of 19.23 and 17.27 nm for as-synthesized $BiVO_4$ and post-reaction, respectively. These average crystallite sizes were determined using the Scherrer eqn (1), indexed to the single-phase monoclinic form of $BiVO_4$, which belongs to the space group $I2/a$ with a lattice constant of a = 5.196 Å, b = 11.704 Å, and c = 5.094 Å according to the joint committee on powder diffraction standards (JCPDS) card no. 04-010-5713. No diffraction peaks from other phases or impurities are observed, indicating high purity and hence a successful synthesis. The position of diffraction peaks of as-synthesized $BiVO_4$ and post-reaction were substantially the same, except for the relative intensity post-reaction peak (112) which decreased, thus indicating that the reaction occurred preferably in that crystalline plane, leading to the dissolution and recrystallization. Possibly, this reduction is related to the formation of Bi-metallic sites on the surface of $BiVO_4$ (Bi–$BiVO_4$).[25] XAS of the as-synthesized $BiVO_4$ and the post-reaction (post-CO_2R) by photoelectrocatalyst under LED illumination as an excitation source were collected at the Bi-L_3 edge. As shown in Fig. 5(B), there are no apparent differences in the spectra suggesting the stability of Bi species in the catalyst by not undergoing chemical transformation. Fig. 5(C) of further analysis of the X-Ray Near Edge Spectra (XANES) reveals a slight left shift (~0.5 eV) in the spectra for the sample post-reaction, likely caused by a local electronic structure effect. Fourier-Transformed Extended X-ray Absorption Fine Structure (FT-EXAFS) shows two main peaks at ~1.7 and 3.0 that are attributed to Bi–O in the first shell and the nearest neighbour Bi–Bi, respectively, as illustrated in Fig. 5(D). A combined effect of localized shortening in the Bi–O bonds and structural expansion of nearest Bi–Bi from bridged BiO_8 (dodecahedral) is observed in the structure

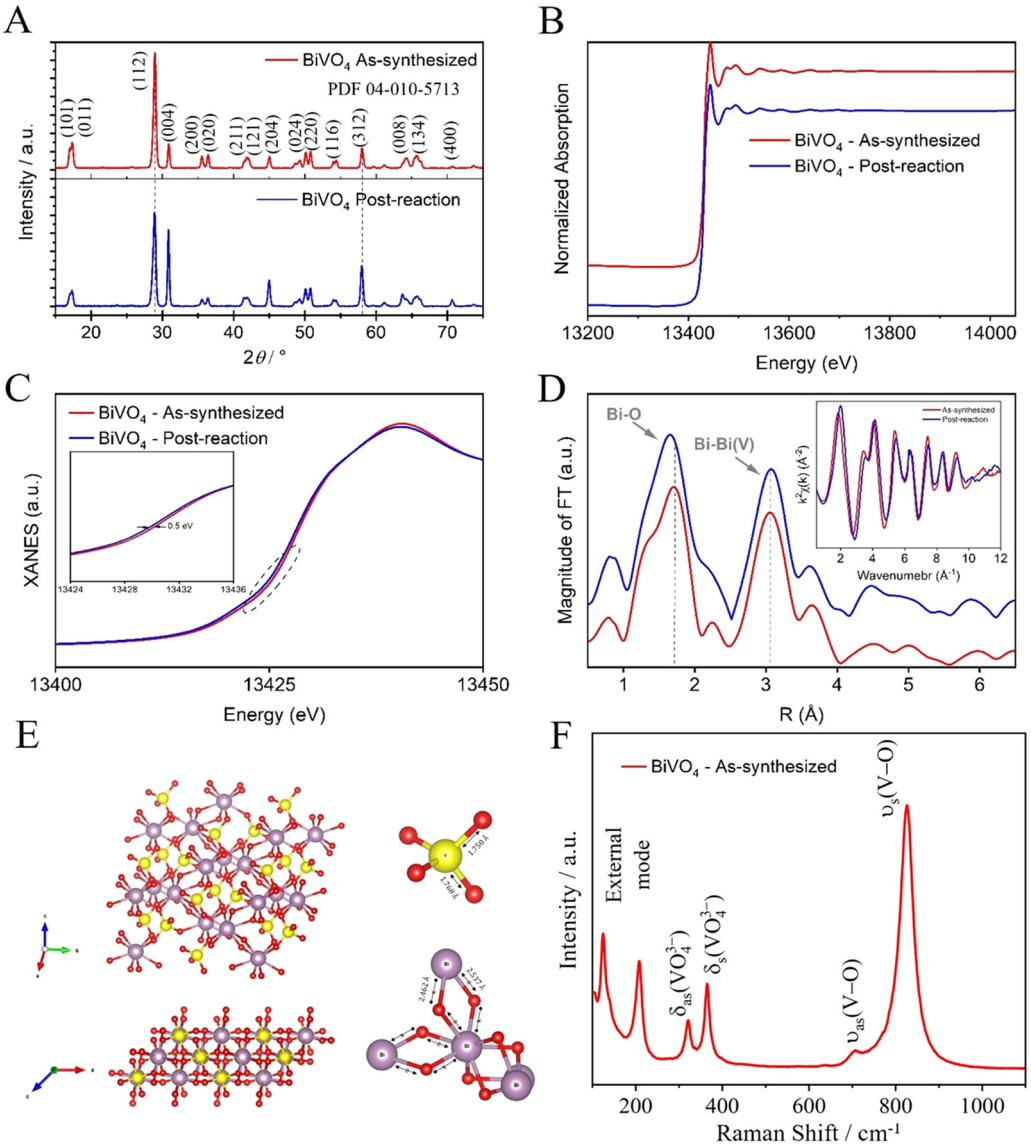

Fig. 5 $BiVO_4$ structural characterization, (A) XRD pattern of the as-synthesized and post-reaction (by photoelectrocatalysis using an LED illumination as an excitation source), (B) XAS spectra of the as-synthesized and post-reaction samples were collected at the Bi-L_3 edge, (C) XANES of the as-synthesized and post-reaction, (D) FT-EXAFS of the as-synthesized and post-reaction, (E) represents monoclinic structure of $BiVO_4$, and (F) Raman spectrum for the as-synthesized $BiVO_4$.

post-reaction. Raman spectroscopy was performed to investigate the short-range order and complement the XRD characterization of the as-synthesized $BiVO_4$, as shown in Fig. 5(F). The Raman bands at around 827, 706, 366, 320, 206, and 124 cm^{-1} are characteristic of the monoclinic $BiVO_4$ phase.[26] The most intense Raman band near 827 cm^{-1} is assigned to the symmetric V–O stretching mode in the crystal structure for the tetrahedral VO_4 groups.[27] The more intense this band, the greater the degree of disorder for average vanadate species. The weak band at 706 cm^{-1} is assigned to the anti-symmetric V–O stretch. The bands near 366 and 320 cm^{-1} are assigned to the symmetric and anti-symmetric deformation modes of the VO_4^{3-} tetrahedral group and the V–O bond, respectively. Finally, the bands near 206 and 124 cm^{-1} are assigned to the external modes (*i.e.*, rotation/translation).[26,28]

It is worth mentioning that some studies have shown a reduction of $BiVO_4$ to bismuthene[29] and its use as an efficient CO_2R.[30,31] Although our experimental conditions could lead to bismuthene formation, the characterization employed did not reveal that transformation. In this sense, despite the bismuthene role should be considered, it is not the only path for CO_2R using $BiVO_4$ as a photoelectrocatalyst. On the other hand, the Bi-metallic formation seems to be essential for CO_2R, as elucidated by the Pourbaix diagrams for Bi.

$BiVO_4$ has demonstrated promising potential as a photoelectrocatalyst as a cathode for CO_2 reduction, meeting several criteria such as the ability to efficiently absorb a wide range of solar spectra, conductive band energy close to driving the CO_2R – which was suppressed by the external potential – least carrier

losses at the interface, and chemical stability. $BiVO_4$ is also a favorable candidate for CO_2R because its synthetic route led to an easy and cost-effective process of scalability, while the required elements are abundant on Earth. Some strategies can be considered in order to increase $BiVO_4$ performance for CO_2R such as its growing as nano-sized particles in the monoclinic phase on the FTO substrate; once there is a resistive force created between the catalyst and the FTO substrate in the PEC system, which reduces the efficiency of the reaction.[19] Growth orientation,[16,32] dopants and/or co-catalysts,[5,33] and heterostructures[34] also can be effective in increasing liquid chemical production.

4. Conclusions

In summary, this study reveals the potential use of $BiVO_4$ as a cathode for photoelectrochemical CO_2R. Assorted reactions were performed by altering the excitation source, by photocatalysis (under different UV and LED illumination), electrocatalysis, and photoelectrocatalysis (using both electrons and photons under UV or LED illumination) sources. Best performances were found to be under photoelectrocatalysis powered by an LED illumination as an excitation source when compared to photocatalysis, electrocatalysis, and photoelectrocatalysis powered by halogen (UV) excitation methods. Photoelectrocatalysis powered by an LED illumination exhibited a total production value of 22 and 5.5 μmol cm^{-2} for methanol and acetic acid, respectively. This is due to the rapid transfer of multiple electrons and protons and the carrier separation possibly promoted by the formation of Bi-metallic sites on the surface of $BiVO_4$ (Bi–$BiVO_4$) and by the externally applied potential, avoiding surface recombination and physical separation. Although $BiVO_4$ as a photocatalyst does not have enough redox potential to drive the CO_2R, the redox potential was adjusted by applying an external potential (at a lower overpotential when compared to electrocatalysis; reducing energy consumption). LED illumination produces higher amounts of products than UV illumination because UV light can interfere with the catalyst surface, affecting the number of catalytic sites available for the reaction. XRD patterns showed the successful synthesis of $BiVO_4$ and the possible formation of Bi-metallic sites on the surface of $BiVO_4$ during CO_2R – formed when a negative potential of −1.0 V *vs.* Ag/AgCl is applied, based on E-pH diagrams from Pourbaix. X-ray Absorption Spectroscopy (XAS) spectra of $BiVO_4$ as-synthesized and post-CO_2R by photoelectrocatalyst under LED illumination excitation showed no apparent differences, suggesting the stability of the Bi species in the bulk catalyst, although on the surfaces these transformations can take place as previously discussed. Thus, this study serves to point out the use of $BiVO_4$ as a cathode for photoelectrochemical CO_2R as well as a critical stepping stone for further studies to improve its performance for energy conversion and assist in advancing sustainable technologies for CO_2 mitigation. Further investigations are required to explore the intricacies of catalyst surfaces.

Conflicts of interest

There are no conflicts to declare.

Acknowledgements

The authors thank Prof. Dr Fernanda de Lourdes Souza and Luis Aparecido de Godoy for their contribution to the discussions of this paper and for their support in the design and construction of the photoelectrochemical reactor, respectively. We thank the Structural Characterization Laboratory (LCE) at the Federal University of São Carlos (UFSCar) for the electron microscopy analyses, the McMaster Analytical X-Ray Diffraction Facility (MAX) for the X-ray diffraction measurements, and the Canadian Light Source (CLS) and the Hard X-ray Microanalysis (HXMA) beamline, where X-ray absorption spectroscopy analysis was carried out. The authors gratefully acknowledge the financial support given by FAPESP (2020/09628-6, 2021/13065-0, 2018/01258-5, 2019/10689-2, 2022/10255-5, 2019/21496-0, 2022/05149-1 2019/21496-0, and 2022/05149-1) and CAPES (Finance Code 001).

References

1 H. Dang, B. Guan, J. Chen, Z. Ma, Y. Chen, J. Zhang, Z. Guo, L. Chen, J. Hu, C. Yi, S. Yao and Z. Huang, *Energy Fuels*, 2024, **38**(6), 4836–4880.
2 P. Chen, Y. Zhang, Y. Zhou and F. Dong, *Nano Mater. Sci.*, 2021, **3**, 344–367.
3 M. Bellardita, V. Loddo, F. Parrino and L. Palmisano, *ChemPhotoChem*, 2021, **5**, 767–791.
4 P. Chen, Y. Zhang, Y. Zhou and F. Dong, *Nano Mater. Sci.*, 2021, **3**, 344–367.
5 L. X. Liu, J. Fu, L. P. Jiang, J. R. Zhang, W. Zhu and Y. Lin, *ACS Appl. Mater. Interfaces*, 2019, **11**, 26024–26031.
6 J. de Almeida, S. H. Câmara, R. Bertazzoli, K. Rajeshwar, R. A. G. da Silva and C. de Arruda Rodrigues, *Chem. Eng. J.*, 2023, **477**, 147117.
7 J. Quiñonero, T. Lana-Villarreal and R. Gómez, *Appl. Catal., B*, 2016, **194**, 141–149.
8 S. S. M. Bhat and H. W. Jang, *ChemSusChem*, 2017, **10**, 3001–3018.
9 O. F. Lopes, K. T. G. Carvalho, A. E. Nogueira, W. Avansi and C. Ribeiro, *Appl. Catal., B*, 2016, **188**, 87–97.
10 R. M. de Silva, F. de Lourdes Souza, E. Dias, G. T. dos, S. T. da Silva, F. E. Durán, A. Rego, D. Higgins and C. Ribeiro, *J. Alloys Compd.*, 2023, **968**, 172090.
11 J. A. Oliveira, R. R. M. Silva, G. T. S. T. da Silva, J. A. Torres, A. Vali, C. Ribeiro, K. Rajeshwar and L. A. M. Ruotolo, *Mater. Res. Bull.*, 2022, **149**, 111716.
12 B. D. Cullity and J. W. Weymouth, *Am. J. Phys.*, 1957, **25**, 394–395.
13 D. L. Wood and J. Tauc, *Phys. Rev. B: Solid State*, 1972, **5**, 3144–3151.
14 O. F. Lopes, K. T. G. Carvalho, W. Avansi, D. M. B. Milori and C. Ribeiro, *RSC Adv.*, 2018, **8**, 10889–10897.

15 H. L. Tan, R. Amal and Y. H. Ng, *J. Mater. Chem. A*, 2017, **5**, 16498–16521.
16 X. Zhu, F. Zhang, M. Wang, X. Gao, Y. Luo, J. Xue, Y. Zhang, J. Ding, S. Sun, J. Bao and C. Gao, *Appl. Catal., A*, 2016, **521**, 42–49.
17 N. Zhang, R. Long, C. Gao and Y. Xiong, *Sci. China Mater.*, 2018, **61**, 771–805.
18 D. Kang, Y. Park, J. C. Hill and K. S. Choi, *J. Phys. Chem. Lett.*, 2014, **5**, 2994–2999.
19 F. Li, W. Zhao and D. Y. C. Leung, *Appl. Catal., B*, 2019, **258**, 117954.
20 Y. Hermans, S. Murcia-López, A. Klein and W. Jaegermann, *ACS Energy Lett.*, 2019, **4**, 2522–2528.
21 J. F. de Brito, P. G. Corradini, M. V. B. Zanoni, F. Marken and L. H. Mascaro, *J. Alloys Compd.*, 2021, **851**, 156912.
22 C. W. Bale and Eve Bélisle, one-metal Eh *vs.* pH Pourbaix diagram.
23 J. Ma, C. Wang and H. He, *Appl. Catal., B*, 2016, **184**, 28–34.
24 T. Li, J. He, B. Peña and C. P. Berlinguette, *Angew. Chem.*, 2016, **128**, 1801–1804.
25 H. Song, J. Sun, T. Shen, L. Deng and X. Wang, *Catalysts*, 2021, **11**(4), 489.
26 M. R. da, S. Pelissari, N. F. Azevedo Neto, L. P. Camargo and L. H. Dall'Antonia, *Electrocatalysis*, 2021, **12**, 211–224.
27 A. Galembeck and O. L. Alves, *J. Mater. Sci.*, 2002, **37**, 1923–1927.
28 S. Nikam and S. Joshi, *RSC Adv.*, 2016, **6**, 107463.
29 W. Ma, J. Bu, Z. Liu, C. Yan, Y. Yao, N. Chang, H. Zhang, T. Wang and J. Zhang, *Adv. Funct. Mater.*, 2021, **31**(4), 2006704.
30 F. Yang, A. O. Elnabawy, R. Schimmenti, P. Song, J. Wang, Z. Peng, S. Yao, R. Deng, S. Song, Y. Lin, M. Mavrikakis and W. Xu, *Nat. Commun.*, 2020, **11**, 1088.
31 C. Cao, D. D. Ma, J. F. Gu, X. Xie, G. Zeng, X. Li, S. G. Han, Q. L. Zhu, X. T. Wu and Q. Xu, *Angew. Chem., Int. Ed.*, 2020, **59**, 15014–15020.
32 G. Xi and J. Ye, *Chem. Commun.*, 2010, **46**, 1893–1895.
33 R. Yalavarthi, R. Zbořil, P. Schmuki, A. Naldoni and Š. Kment, *J. Power Sources*, 2021, **483**, 229080.
34 N. Khan, F. Stelo, G. H. C. Santos, L. M. Rossi, R. V. Gonçalves and H. Wender, *Appl. Surf. Sci.*, 2022, **11**, 100289.